Pergamon

Int. J. Solids Structures Vol. 33, No. 5, pp. 629–645, 1996

0020-7683/96 $9.50 + .00

0020-7683(95)00064-X

FULLY-PLASTIC CRACK PROPAGATION IN STIFFENED PLATES

MICHELLE S. HOO FATT
Department of Ocean Engineering, Massachusetts Institute of Technology, Cambridge, MA 02139, U.S.A.

(*Received* 19 *June* 1994; *in revised form* 6 *March* 1995)

Abstract—The detachment of a stiffener from a plate is described by the fully-plastic crack propagation in the web of a non-symmetric I-beam. The lower flange of the non-symmetric I-beam represents the effective plate width, which may peel away from the stiffener. By assuming a rigid, linear strain-hardening material, we distinguish between two responses of the lower flange depending on the load amplitude: deformation without crack growth and deformation with crack growth. The bifurcation point that marks the transition from a deformation without crack growth to deformation with crack growth is independent of the initial crack length, but depends on the relative magnitude of plastic modulus to the material flow stress, the specific work of fracture, and the relative size of the tear zone and width of the flange. A parametric study shows that bifurcation load increases approximately linearly with an increasing ratio of web to flange widths for some chosen material constants. The effective width of the stiffened plate is thus an important parameter in the detachment of the plate from the stiffener.

1. INTRODUCTION

The problem associated with tearing in structures composed of stiffened panels is addressed in this paper. The detachment of the plate from the stiffener due to crack propagation in the stiffener web usually takes place at or above the heat-affected zone of the weldment. Because most structures are designed to operate at loads several times below their limit load, fracture and crack growth which may be induced by accidental loading occurring in the presence of large plastic deformation. Conventional techniques from elastic fracture mechanics cannot be used for solving this type of problem. We can, however, use simple energy and equilibrium methods to examine the load–deflection and crack growth characteristics of the structure as it undergoes steady-state crack propagation or peeling. This simple engineering approach for dealing with the steady-state tearing of metals has given accurate solutions to predict the tearing loads associated with adhesives fracture [see Atkins and Mai (1985)], and in recent years has been applied to problems involving cohesive fractures (Atkins and Liu, 1993; McClintock, 1994). According to Chang *et al.* (1972), the difference between adhesive and cohesive fractures is in the specific work that is required to create a new adhesive or cohesive surface area as the crack propagates.

Equilibrium of a linear strain-hardening beam and the principle of virtual work are combined to find the deformation characteristic of the detached panel. The rigid, linear-strain hardening material assumption is distinguished from the non-hardening model proposed by McClintock (1994) in earlier attempts to understand fully-plastic fracture of welded T-joints. The strain-hardening material assumption is not only needed to find how the plastic modulus affects crack propagation, but also gives a more accurate representation of the behavior of structures which strain-harden during plastic flow [see Youngdahl (1991)]. The results of this study should give an insight into the fracture process and provide simple analytical tools that may be used for the prevention of crack growth in stiffened structures.

2. PROBLEM FORMULATION

Consider a crack of initial length $2a_0$ in the stiffener web of a non-symmetric I-beam. The lower flange of the non-symmetric I-beam may represent an effective plate width

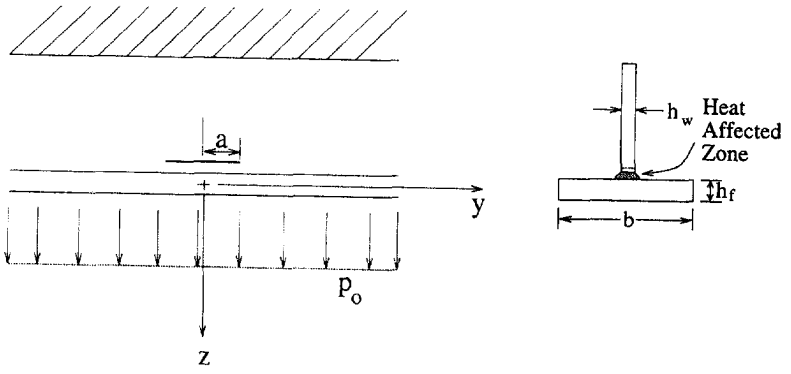

Fig. 1. Geometry of a non-symmetric I-beam with crack in the stiffener web.

associated with the stiffener. Both the upper flange and web of the stiffener are fixed and considered rigid as shown in Fig. 1. A transverse load on the lower flange (or plate) causes it to peel away from the stiffener. This type of tearing occurs when there is an initial crack in the stiffener web, usually in or above the heat-affected zone of the weldment. Denote the web and lower flange thickness as h_w and h_f, respectively. The initial crack of length a_0 is centered at mid-length, $y = 0$. A uniform load p_0 is applied over the entire length of the lower flange such that, locally, the lower flange of the beam is bent in the region $|y| < a$. Here the crack length a will be greater than a_0 if the crack propagates.

2.1. *Assumptions*

We make the following set of assumptions.

(1) Extensive plastic deformation occurs before and during crack propagation.

(2) Elastic effects are negligible and the material behavior is rigid, linear strain-hardening.

(3) The transverse shear stress is small and does not influence plastic yielding or crack propagation. This restricts the initial crack length to be greater than 10 times its thickness.

(4) In the case of crack growth, we shall assume that the process zone is small† so that the specific work to fracture or fracture resistance, R, is taken as the elastic fracture resistance, a known material quantity that can be found in the literature or from experiments.

2.2. *Transition between deformation and crack growth*

As the material is rigid–plastic, a minimum load is required for plastic deformation to occur. Above this minimum load is a critical load at which steady-state crack growth will begin to take place [see Atkins and Liu (1993)]. If the bending moment at the crack tip is less than the critical moment to cause steady-state crack propagation, M_{cr}, but greater than that to cause plastic flow, $M_0 = \sigma_0 h^2/4$, the flange will deflect without crack propagation. We can therefore distinguish between two modes of deformation: (1) deformation without crack growth, i.e. deflection of the lower flange without crack propagation; and (2) deformation with crack growth, i.e. deflection of the lower flange coupled with extension of the crack. The particular type of deformation mode depends on the load amplitude as well as the geometry and material properties of the beam.

3. CURVATURE AT CRACK TIP FOR QUASI-STATIC CRACK PROPAGATION

The moment (and corresponding curvature) at the crack tip is constant during steady-state crack propagation [see Atkins and Mai (1985)]. A control volume incorporating the

†The size of the process zone is usually larger in plastic fractures when compared with elastic ones because of localized necking at the crack tip. However, Atkins and Mai (1985) found particular cases of fully-plastic crack growth in which the process zone is small, comparable with those in elastic fracture.

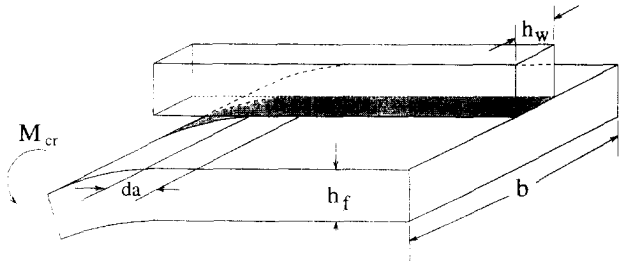

Fig. 2. Inside the control volume at the crack tip.

tear zone with enough material on either side of the crack for steady-state tearing has been proposed by McClintock (1994) in evaluating the critical moment and curvature of a related problem, the peeling of welded T-joints. We will use a similar approach to calculate M_{cr} and κ_{cr} for this problem.

Using the principle of virtual work, one can state the following expression during steady-state crack propagation in the control volume shown in Fig. 2:

$$dW = d\Gamma + R\,dA, \tag{1}$$

where dW is the increment in external work, $d\Gamma$ is plastic work increment, R is the specific work of fracture in the presence of extensive plastic flow [see Atkins and Mai (1985)] and dA is the incremental crack area.

The incremental plastic work $d\Gamma$ to bend the flange at the crack tip is

$$d\Gamma = 2b\int_0^{da}\int_0^{h_f/2}\int_0^{\varepsilon}\sigma\,d\varepsilon\,dz\,ds. \tag{2}$$

Substituting $\sigma = \sigma_0 + E_p\varepsilon$ and integrating with respect to $d\varepsilon$ gives

$$d\Gamma = 2b\int_0^{da}\int_0^{h_f/2}\left(\sigma_0\varepsilon + \frac{E_p\varepsilon^2}{2}\right)dz\,ds. \tag{3}$$

Using $\varepsilon = z\kappa$ gives the increment in plastic work

$$d\Gamma = \frac{bh_f^2\kappa\,da}{24}(6\sigma_0 + E_p h_f\kappa). \tag{4}$$

The increment in work to tear a crack of length da is

$$dT = Rh_w\,da. \tag{5}$$

If we denote a critical bending moment to tear the crack as M_{cr}, then the work increment that is needed to tear and plastically deform the beam is

$$dW = M_{cr}\kappa_{cr}\,da. \tag{6}$$

where M_{cr} is the bending moment corresponding to κ_{cr}.

From the principle of virtual work as expressed in eqn (1), one obtains

$$M_{cr}|_{\kappa_{cr}} = \frac{bh_f^2\kappa_{cr}}{24}(6\sigma_0 + E_p h_f \kappa_{cr}) + Rh_w. \tag{7}$$

We can also express M_{cr} in terms of κ_{cr} because the two are related for a rigid, linear strain-hardening material

$$M_{cr} = \frac{bh_f^2\sigma_0}{4} + \frac{bh_f^3 E_p \kappa_{cr}}{12}. \tag{8}$$

Equating both expressions for M_{cr} in eqns (7) and (8) gives

$$\left[\frac{bh_f^2\sigma_0}{4} + \frac{bh_f^3 E_p \kappa_{cr}}{12}\right]_{\kappa_{cr}} = \frac{bh_f^2\kappa_{cr}}{24}(6\sigma_0 + E_p h_f \kappa_{cr}) + Rh_w. \tag{9}$$

From eqn (9), we obtain an expression for κ_{cr}:

$$\kappa_{cr} = \frac{24Rh_w}{bh_f^3 E_p}. \tag{10}$$

We can also substitute this expression into eqn (8) to evaluate M_{cr}

$$M_{cr} = \frac{bh_f^2\sigma_0}{4} + \frac{bh_f^2 E_p}{12}\sqrt{\left(\frac{24Rh_w}{bh_f^3 E_p}\right)}. \tag{11}$$

Equations (10) and (11) give the critical curvature and bending moment at the bend during crack growth.

4. TYPE I: DEFORMATION WITHOUT CRACK GROWTH

The bending moment distribution along a fixed-end beam subject to uniform transverse load is shown in Fig. 3. Note that the bending moment is maximum at the crack tip and at the center of the flange. These are thus regions where plastic flow will first occur in a bent rigid–plastic flange. Even though the elastic bending stresses at the crack tip are twice the magnitude of those at the center of the flange, plastic flow must occur simultaneously at both locations. This is because a deformation mechanism that is plastically deforming at both crack tips yields finite slopes of the rigid portion of the flange and the only way this

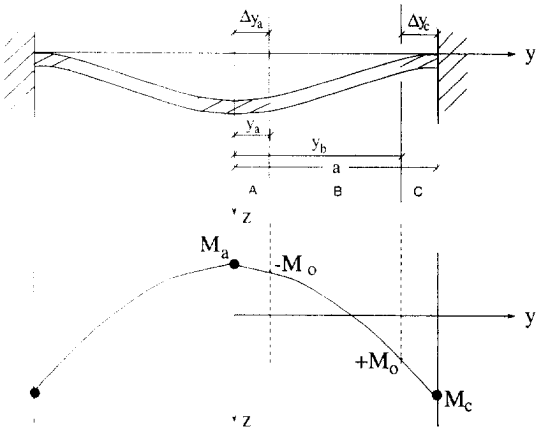

Fig. 3. Distributed bending moments and plastic regions.

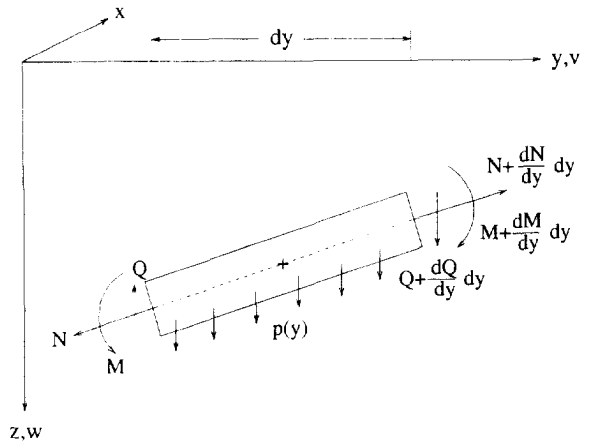

Fig. 4. Free-body diagram of a differential beam element.

mechanism may be admissible is if the curvature is reversed at the center of the beam. Thus, a plastic region of opposite curvature must occur simultaneously at the center of the beam.

There are three distinct regions of the half flange shown in Fig. 3, A, B, and C. The flange plastically deforms in regions A and C with associated plastic zone sizes Δy_a and Δy_c, respectively, and it remains rigid in region B. We denote the distance to the end of region A y_a and the distance to the end of region B y_b. With this plastic mechanism for the linear strain-hardening flange, we can derive expressions for the deflection profile by satisfying equilibrium, the rigid–plastic constitutive relationships, and boundary or continuity conditions.

4.1. *Equilibrium*

Recall from classical beam theory that the equilibrium equations corresponding to the differential element of the flange shown in Fig. 4 is as follows:

$$\Sigma F_y = 0 \Rightarrow \quad \frac{dN}{dy} = 0 \tag{12}$$

$$\Sigma M_x = 0 \Rightarrow \quad \frac{dM}{dy} = -Q \tag{13}$$

and

$$\Sigma F_z = 0 \Rightarrow \quad \frac{d^2M}{dy^2} + \frac{d}{dy}\left(\frac{N\,dw}{dy}\right) - p = -\frac{dQ}{dy} + \frac{d}{dy}\left(\frac{N\,dw}{dy}\right) - p = 0, \tag{14}$$

where N is the membrane force and M is the bending moment in the beam.

4.2. *Plastic constitutive relations*

For a linear strain-hardening material, the bending moment M is given by

$$M = M_0 + \bar{E}_p \kappa, \tag{15}$$

where $\bar{E}_p = E_p b h_f^3/12$, and the axial force N is

$$N = N_0 + E_p \varepsilon_0. \tag{16}$$

We shall restrict our analysis to infinitesimal deflection, i.e. $N = 0$.

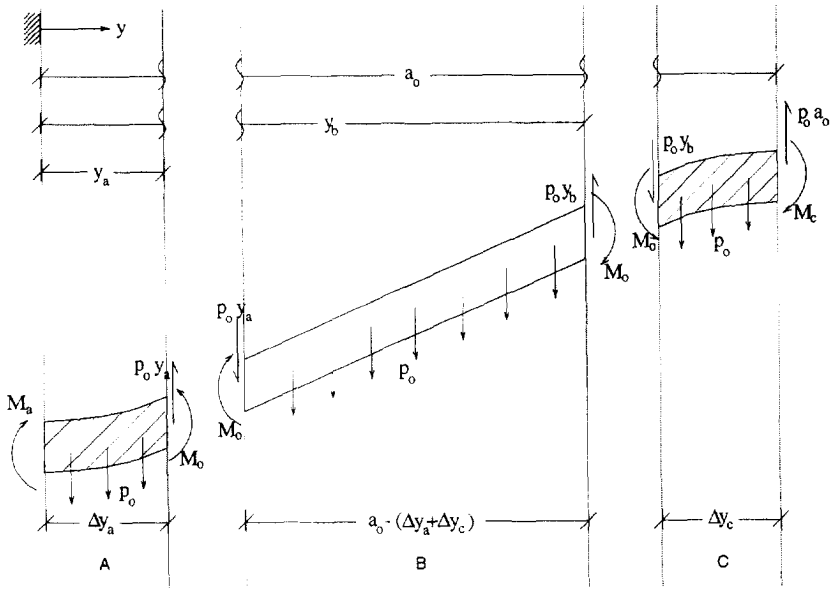

Fig. 5. Free-body diagram of regions A, B and C within the plastic flange.

Membrane forces not only stiffen the beam when its deflections are greater than a few times its thickness [see Haythornwaite (1961)], but they can also influence the fracture mode. In analyzing the problem of flow with crack propagation we have assumed propagation to be type I (tensile opening). Membrane forces will cause the crack to propagate in both mode I and mode II (shear mode).

4.3. *Boundary and continuity equations*

The boundary and continuity conditions for the three regions of the fixed-end flange shown in Fig. 5 are

$$Q(0) = 0 \tag{17}$$

$$\frac{dw}{dy}(0) = 0 \tag{18}$$

$$[w]_{y_a} = [w]_{y_b} = 0 \tag{19}$$

$$\left[\frac{dw}{dy}\right]_{y_a} = \left[\frac{dw}{dy}\right]_{y_b} = 0 \tag{20}$$

$$w(a) = 0 \tag{21}$$

and

$$\frac{dw}{dy}(a) = 0, \tag{22}$$

where square brackets denote a jump discontinuity of the value within the brackets. Equations (19) and (20) therefore show that the slope and deflection are continuous at the boundaries of regions A, B and C.

4.4. *Region A*

The bending moment in this region is found by setting $N = 0$ in the equilibrium equation given by eqn (14) and integrating it with respect to y

$$Q = -p_0 y + a_1, \tag{23}$$

where a_1 is a constant. Satisfying the boundary condition in eqn (17) gives $a_1 = 0$. Substituting this result into eqn (13), one obtains

$$M = \frac{p_0 y^2}{2} + a_2. \tag{24}$$

A more elegant solution for the bending moment can be obtained if we express a_2 in terms of the distance between the centerline and the end of the central plastic zone or the half-size of the central plastic zone, $y_a = \Delta y_a$. A relationship between a_2 and y_a is found by using the condition that $M(y_a) = -M_0$ or by requiring moment equilibrium of the entire plastic region y_a in the flange (see Fig. 5)

$$a_2 = -M_0 - \frac{p_0 y_a^2}{2}. \tag{25}$$

Substituting eqn (25) into eqn (24) gives the bending moment in terms of y_a

$$M = \frac{p_0 (y^2 - y_a^2)}{2} - M_0. \tag{26}$$

Note that the curvature of region A, $\kappa = d^2w/dy^2$, is negative in Fig. 4. The appropriate constitutive relationship describing the moment-curvature relationship in this region is

$$M = -M_0 + \bar{E}_p \kappa. \tag{27}$$

Substituting eqn (26) into eqn (27) gives an expression for the curvature in this region:

$$\bar{E}_p \frac{d^2 w}{dy^2} = \frac{p_0 (y^2 - y_a^2)}{2}. \tag{28}$$

Integrating eqn (28) with respect to y and satisfying the boundary condition in eqn (18) gives

$$\bar{E}_p \frac{dw}{dy} = \frac{p_0}{2}\left(\frac{y^3}{3} - y_a^2 y\right). \tag{29}$$

Integrating eqn (29) again with respect to y gives

$$\bar{E}_p w = \frac{p_0}{2}\left(\frac{y^4}{12} - \frac{y_a^2 y^2}{2}\right) + a_4, \tag{30}$$

where a_4 is a constant that may be evaluated from the continuity relations.

4.5. *Region B*

The flange deforms as a rigid body in region B, i.e. rigid body rotation and translation. The constant slope of the flange is

$$\bar{E}_p \frac{dw}{dy} = b_1, \tag{31}$$

while the deflection is given by

$$\bar{E}_p w = b_1 y + b_2, \tag{32}$$

where b_1 and b_2 are constants.

4.6. *Region C*

The bending moment in this region is also found by taking moments at a particular cross-section in region C (see Fig. 5). This gives

$$M = M_0 + p_0 y_b (y - y_b) + \frac{p_0}{2}(y - y_b)^2. \tag{33}$$

The curvature $\kappa = d^2w/dy^2$ in A is positive, and the moment-curvature relationship describing of the flange in this region is

$$M = M_0 + \bar{E}_p \kappa. \tag{34}$$

Substituting eqn (33) into eqn (34), one finds an expression for $\bar{E}_p d^2w/dy^2$ in terms of y_b

$$\bar{E}_p \frac{d^2 w}{dy^2} = \frac{p_0}{2}(y^2 - y_b^2). \tag{35}$$

We conveniently expressed the bending moment in terms of the distance between the centerline and the start of the plastic zone at the crack tip y_b. Integrating eqn (35) twice with respect to y gives

$$\bar{E}_p \frac{dw}{dy} = \frac{p_0}{2}\left(\frac{y^3}{3} - y_b^2 y\right) + c_3 \tag{36}$$

and

$$\bar{E}_p w = \frac{p_0}{2}\left(\frac{y^4}{12} - y_b^2 \frac{y^2}{2}\right) + c_3 y + c_4, \tag{37}$$

where c_3 and c_4 are constants.

4.7. *Load–deflection characteristics*

The solution for the deflection profile throughout the flange is described by the following unknown quantities: y_a, a_4, b_1, b_2, y_b, c_3 and c_4. Four of these can be determined from the boundary conditions described in eqns (20)–(22). The missing equations are found via moment equilibrium condition of the rigid portion of the beam, region B in Fig. 5. This gives

$$\frac{4M_0}{p_0} = y_b^2 - y_a^2. \tag{38}$$

Another equation results from the condition that the slopes at $y = y_a$ and at $y = y_b$ are the same. The latter condition gives

$$\left[\frac{dw}{dy}\right]_{y_a} = \left[\frac{dw}{dy}\right]_{y_b} = 0 \tag{39}$$

or

$$-2y_a^3 = -2y_b^3 + 3ay_b^2 - a^3. \tag{40}$$

A simple closed-form expression for y_a and y_b cannot be obtained from eqns (38) and (40) because of the cubic relation between y_a and y_b in eqn (40).

The above set of equations involving the unknown quantities can be solved, and expressions for the unknown constants of integration are

$$b_1 = \frac{-p_0 y_a^3}{3} \tag{41}$$

$$b_2 = \frac{-5p_0 y_b^4}{24} + \frac{p_0}{24}[12ay_b^3 - 6a^2 y_b^2 + (8y_a^3 - 4a^3)y_b + 3a^4] \tag{42}$$

$$a_4 = \frac{-p_0 y_a^4}{8} + b_2 = \frac{-p_0 y_a^4}{8} + \frac{-5p_0 y_b^4}{24} + \frac{p_0}{24}[12ay_b^3 - 6a^2 y_b^2 + (8y_a^3 - 4a^3)y_b + 3a^4] \tag{43}$$

$$c_3 = \frac{p_0}{6}[3ay_b^2 - a^3] \tag{44}$$

and

$$c_4 = \frac{p_0}{8}[a^4 - 2a^2 y_b^2]. \tag{45}$$

Equations (30), (32) and (37), with the integration constants listed above, describe the deflection profile of the flange.

The central deflection of the beam is denoted $w_p = w(0)$ and is evaluated from eqn (30) as

$$\bar{E}_p w_p = a_4 = \frac{-p_0 y_a^4}{8} + \frac{-5p_0 y_b^4}{24} + \frac{p_0}{24}[12ay_b^3 - 6a^2 y_b^2 + (8y_a^3 - 4a^3)y_b + 3a^4]. \tag{46}$$

The deflection profile of the beam has been written in terms of y_a and y_b, where the values of y_a and y_b depend on the load and geometry of the flange.

5. TYPE II: DEFORMATION WITH CRACK GROWTH

After reaching a critical moment M_{cr}, the material tears at the crack tip and unloads as the crack propagates. The force–deflection characteristics of the flange exhibiting type II behavior now depend on unloading at the crack tip; because unloading is such an important aspect of the solution, it will be explained in the following section.

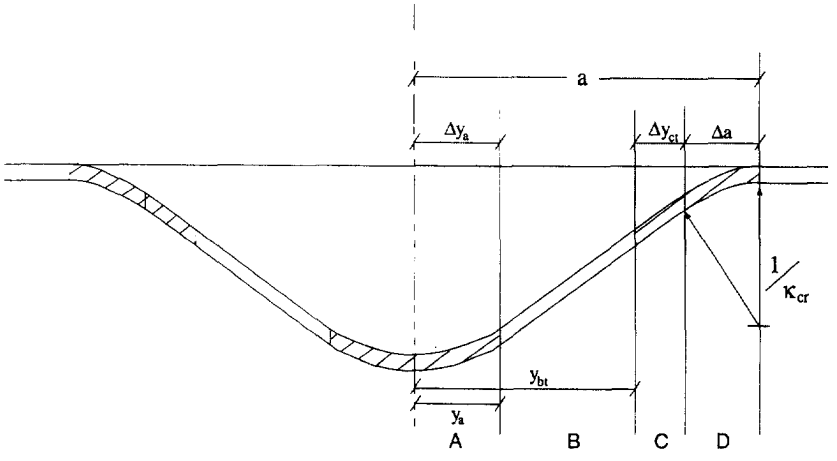

Fig. 6. Deformation field of plastic flange during crack growth.

5.1. *Plastic unloading and loading regions*

Figure 6 shows the deflection profile of the flange as the crack propagates in quasi-steady state. There are two unloading regions: (1) region D in which the crack extends by Δa; and (2) region C, a plastic region of constant length Δy_{ct}. Because we have assumed the material to be rigid–plastic, the unloading path of the material in the Δa region is represented by a vertical line as shown in Fig. 7. This unloading path signifies that, while the crack extends, the bending moment in the unloaded region adjacent to the crack tip decreases from M_{cr}, while the curvature of the flange remains at a constant value equal to κ_{cr}. We denote the moment at the end of region C as M_c.

The size of the second plastic region, region C, must remain constant during crack growth because the material here is also unloading. Only loaded regions can grow. The constant value of Δy_{ct} corresponds to that of Δy_c when a transition from type I to type II has just occured. Each material point in region C unloads with a constant curvature to some value of the moment that can be found through moment equilibrium in this region (vertical lines in Fig. 7). The trajectory of the bending moment at each position corresponding to the curvatures shown in Fig. 7 will depend on the amount of crack extension Δa.

Denote the distance to the end of regions A and B at the transition of type I to type II behavior as y_{at} and y_{bt}, respectively. As the crack propagates, material in region A may continue to be in a loading region even though region C is an unloading region.

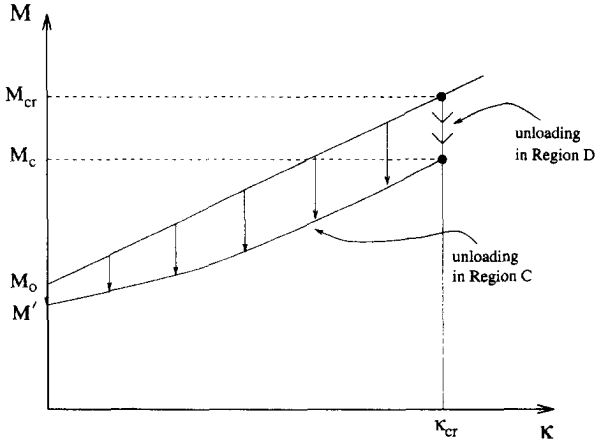

Fig. 7. Plastic unloading of regions C and D.

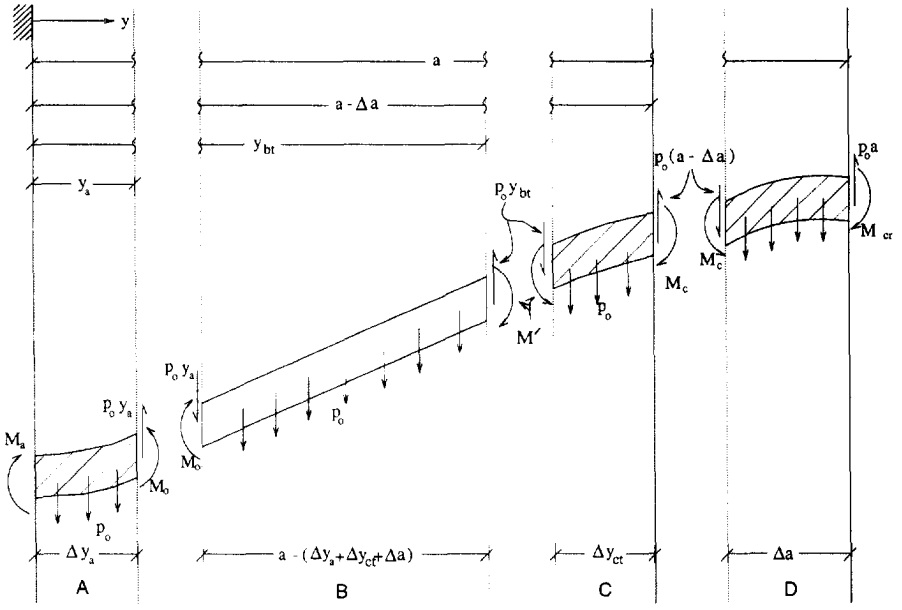

Fig. 8. Free-body diagram of regions A, B, C and D within the plastic flange during crack growth.

The unloading and loading regions described above give a free-body diagram of the flange in type II as shown in Fig. 8. This is similar to that in type I, except for the region of crack extension Δa and the region of constant length Δy_{ct}. Because Δy_{ct} unloads to a reduced bending moment during unloading, the bending moment at the location of the rigid portion of the beam M' is related to the crack growth Δa:

$$M' = M_{cr} + \frac{p_0(\Delta y_{ct} + \Delta a)^2}{2} - p_0 a(\Delta y_{ct} + \Delta a). \tag{47}$$

5.2. *Boundary conditions*

A solution for deflection of the flange in regions A and B is subject to a new set of displacement and slope boundary conditions that are prescribed at $y = y_{bt}$. The slope and deflection at $y = y_{bt}$ consist of two parts due to additional curling of region D as the crack propagates and the slope and deflection at the point of transition from type I to type II. The latter components for the slope and deflection are derived from the previous type I solution. The region defined by length Δy_{ct} undergoes rigid body translation and rotation due to additional curling of Δa.

5.2.1. *Curling.* We shall denote the deflection and slope at $y = a - \Delta a$ due to additional curling by subscript c. Using small angle approximations, one finds the following expressions for w_c and $(dw/dy)_c$:

$$w_c \approx \frac{\kappa_{cr}(\Delta a)^2}{2} \tag{48}$$

and

$$\left(\frac{dw}{dy}\right)_c \approx \kappa_{cr}\Delta a. \tag{49}$$

5.2.2. *Fixed transitional values.* All quantities at the transition from type I to type II will be denoted by subscript t. We can calculate the slope and deflection at the point of transition by using the previous type I solution. The deflection w_t and slope $(dw/dy)_t$,

however, depend on the values of y_a, y_b and p_0 which are expressed implicitly by eqns (38) and (40) as well as the value of Δy_{ct} calculated from the moment equilibrium of region C when $M_c = M_{cr}$ (see Fig. 5). Requiring equilibrium of moments for this region gives a relation between M_{cr} and Δy_{ct}:

$$M_{cr} = M_0 + \frac{p_t \Delta y_{ct}}{2}(2a_0 - \Delta y_{ct}), \tag{50}$$

where $\Delta y_{ct} = a_0 - y_{bt}$. Here we have denoted a transitional load p_t to represent the load at which a change from type I to type II occurs. The values of y_{at} and y_{bt} are found from eqns (38) and (40)

$$\frac{4M_0}{p_t} = y_{bt}^2 - y_{at}^2 \tag{51}$$

and

$$-2y_{at}^3 = -2y_{bt}^3 + 3a_0 y_{bt}^2 - a_0^3. \tag{52}$$

Equations (50)–(52) give an implicit representation of p_t, y_{at} and y_{bt}.

The solution for the transitional deflection w_t is obtained from eqn (37):

$$\bar{E}_p w_t = \frac{p_t}{24}[-5y_{bt}^4 + 12a_0 y_{bt}^3 - 6a_0^2 y_{bt}^2 - 4a_0^3 y_{bt} + 3a_0^4], \tag{53}$$

while the transitional slope $(dw/dy)_t$ is obtained from eqn (36):

$$\bar{E}_p\left(\frac{dw}{dy}\right)_t = \frac{-p_t y_{at}^3}{3}. \tag{54}$$

Note that the crack length at the transition point is a_0. The initial crack length should be distinguished from the crack length during crack growth, a.

5.3. *Load–deflection characteristics*

The general equations used to describe the deflection profile $\bar{E}_p w$ and slope $\bar{E}_p dw/dy$ of the flange in regions A and B are of identical form to those derived in the previous type I solution, but the values of the integration constant a_4, b_1 and b_2 are different because we require different slope and displacement boundary conditions at $y = y_{bt}$.

As in the previous case, satisfying slope continuity at $y = y_a$, eqn (20), gives a relation for b_1

$$b_1 = \frac{-p_0 y_a^3}{3}. \tag{55}$$

We require displacement continuity at $y = y_{bt}$, eqn (19), to obtain a new expression for b_2

$$b_2 = \frac{p_0 y_a^3}{3} y_{bt} + \frac{p_t}{24}[-5y_{bt}^4 + 12a_0 y_{bt}^3 - 6a_0^2 y_{bt}^2 - 4a_0^3 y_{bt} + 3a_0^4] + \frac{\bar{E}_p \kappa_{cr}(\Delta a)^2}{2}. \tag{56}$$

The value of a_4 is derived from the condition of displacement continuity at $y = y_a$, eqn (19), and it is identical to the expression for it in type I [see eqn (44)].

The equation for the central deflection of the flange is obtained from eqn (30) with the new expressions for a_4 and b_2

$$\bar{E}_p w = \frac{p_0}{24}[-3y_a^4 + 8y_a^3 y_{bt}] + \frac{p_1}{24}[-5y_{bt}^4 + 12a_0 y_{bt}^3 - 6a_0^2 y_{bt}^2 - 4a_0^3 y_{bt} + 3a_0^4] + \frac{\bar{E}_p \kappa_{cr}(\Delta a)^2}{2}. \tag{57}$$

Equation (58) is expressed in terms of y_a and Δa. We can find an equation relating these two values by equating the slope boundary conditions prescribed at $y = y_a$ and $y = y_{bt}$. Thus the expression given in eqn (55) is equal to the sum of those specifed by eqns (49) and (54)

$$\frac{p_0 y_a^3}{3} = \frac{p_1 y_{at}^3}{3} + \bar{E}_p \kappa_{cr} \Delta a. \tag{58}$$

Another equation relating y_a to Δa comes from the moment equilibrium of the rigid portion of the beam, region B in Fig. 8:

$$M_0 + M' = \frac{p_0}{2}(y_{bt}^2 - y_a^2). \tag{59}$$

Substituting the expression for M' in eqn (47) into eqn (59) gives

$$M_0 + M_{cr} = \frac{p_0}{2}(a^2 - y_a^2), \tag{60}$$

where $a = a_0 + \Delta a$. By setting $\Delta a = 0$ in the above system of equations, eqns (58), (58) and (60), one retrieves the same solution for the central deflection at the point of transition from type I to type II. A bifurcation point is obtained at the transition from type I to type II behavior.

6. DISCUSSION OF RESULTS

We introduce the following dimensionless quantities:

$\bar{m} = M/M_0$, bending moment;
$\bar{p} = p_0 a_0^2/4M_0$, load amplitude;
$\bar{w}_p = w_p/h_f$, deflection at centerline;
$\bar{y}_a = y_a/a_0$, distance of plastic zone at center of flange;
$\bar{y}_b = y_b/a_0$, distance to plastic zone at crack tip;
$\Delta\bar{a} = \Delta a/a_0$, crack growth;
$\Delta\bar{y}_a = \Delta y_a/a_0$, plastic zone size at center of flange;
$\Delta\bar{y}_c = \Delta y_c/a_0$, plastic zone size at crack tip;
$\bar{\kappa} = h_f\kappa$, curvature;
$\eta = a_0/h_f$, initial crack length parameter;
$\lambda = b/h_f$, stiffener footing parameter;
$\mu = h_w/b$, tear zone parameter;
$\zeta = E_p/\sigma_0$, ratio of plastic modulus to flow stress;
and $r = 24R/h_w E_p$, specific work of fracture parameter.

6.1. *Type* I

Equations (40), (38) and (46) are expressed in terms of the normalized or dimensionless parameters as follows:

$$-2\bar{r}_a^3 = -2\bar{r}_b^3 + 3\bar{r}_b^2 - 1 \tag{61}$$

$$\bar{p} = \frac{1}{\bar{r}_b^2 - \bar{r}_a^2} \tag{62}$$

and

$$\bar{w}_p = \frac{\bar{p}\eta^2}{2\zeta}[-3\bar{r}_a^4 - 5\bar{r}_b^4 + 12\bar{r}_b^3 - 6\bar{r}_b^2 + 4(2\bar{r}_a^3 - 1)\bar{r}_b + 3]. \tag{63}$$

Substituting the expression for $2\bar{r}_a^3$ in eqn (61) into eqn (63), one finds

$$\bar{w}_p = \frac{\bar{p}\eta^2}{2\zeta}[-3\bar{r}_a^4 + 3\bar{r}_b^4 - 6\bar{r}_b^2 + 3] = \frac{3\bar{p}\eta^2}{2\zeta}[-\bar{r}_a^4 + (1-\bar{r}_b^2)^2]. \tag{64}$$

Although we are only concerned with how the beam deflection varies with the applied load, it is worth mentioning some interesting features of the solution obtained by assuming a rigid, linear strain-hardening beam. First, the sizes of the plastic zones are fully described by eqns (61) and (62) and depend only on the normalized load $\bar{p}$. The plastic zone sizes are independent of ζ or the plastic modulus E_p. This result may seem counter-intuitive because one might expect that the degree of strain-hardening would affect the size of the plastic zones. In this case, it does not. Secondly, it can be shown that the magnitude of the bending moment at the crack tip is always less than that at the center of the flange. In a rigid, perfectly-plastic beam, both moments are of equal magnitude but opposite signs. In an elastic beam, one finds that the bending moment at the crack tip is twice that at the center of the beam.

6.2. *Type* II

The normalized critical curvature and bending moment at the crack tip are

$$\bar{\kappa}_{cr}^2 = r\lambda\mu^2 \tag{65}$$

and

$$\bar{m}_{cr} = 1 + \frac{\zeta\mu}{3}\sqrt{r\lambda}, \tag{66}$$

respectively.

The following expressions are the normalized system of equations:

$$\bar{p}\bar{r}_a^3 = \bar{p}_1\bar{r}_{at}^3 + \frac{\zeta\bar{\kappa}_{cr}\Delta\bar{a}}{4} \tag{67}$$

$$\bar{p} = \frac{(1+\bar{m}_{cr})}{2[(1+\Delta\bar{a})^2 - \bar{r}_a^2]} \tag{68}$$

and

$$\bar{w}_p = \frac{\eta^2\bar{p}}{2\zeta}[-3\bar{r}_a^4 - 8\bar{r}_a^3\bar{r}_{bt}] + \frac{\eta^2\bar{p}_1}{2\zeta}[-5\bar{r}_{bt}^4 + 12\bar{r}_{bt}^3 - 6\bar{r}_{bt}^2 - 4\bar{r}_{bt} + 3] + \frac{\eta^2\bar{\kappa}_{cr}(\Delta\bar{a})^2}{2}, \tag{69}$$

where the normalized transitional values are

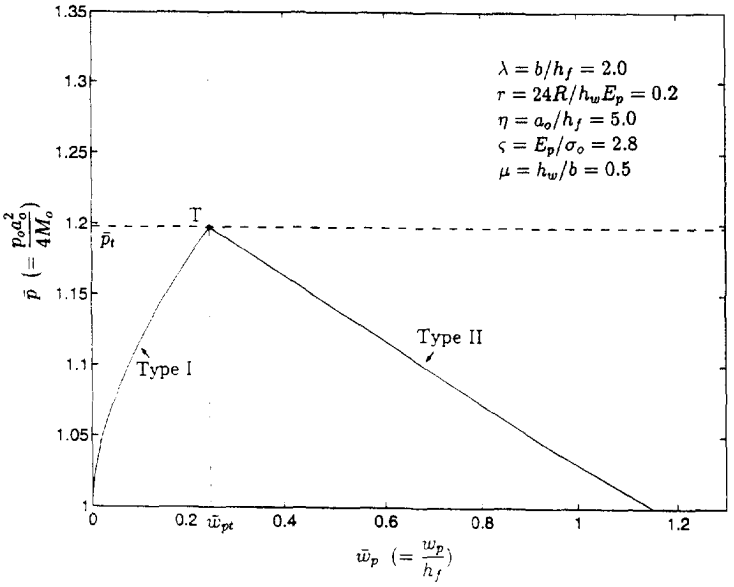

Fig. 9. Bifurcation point between deformation without crack growth (type I) and deformation with crack growth (type II).

$$\bar{m}_{cr} = 1 + 2\bar{p}_t(1 - \bar{r}_{bt}^2) \tag{70}$$

$$\bar{p}_t = \frac{1}{\bar{r}_{bt}^2 - \bar{r}_{at}^2} \tag{71}$$

and

$$-2\bar{r}_{at}^3 = -2\bar{r}_{bt}^3 + 3\bar{r}_{bt}^2 - 1. \tag{72}$$

The beam deflection now depends not only on the same material parameters as in Section 4, but also on the value of the $\bar{\kappa}_{cr}$ or $\bar{m}_{cr}$. These in turn depend on the specific work to fracture parameter $r = 24R/h_w E_p$ and a stiffener footing parameter $\lambda = b/h_f$.

6.3. *Transition from type* I *to type* II

As an example, the material properties for mild steel given in Table 1 are used to evaluate the material parameters. The thickness of the web or the width of the tear zone is taken to be $h_w = 0.032$ m, a typical value that is found in most applications. With this, one finds that $\varsigma = E_p/\sigma_0 = 2.8$ and $r = 24R/h_w E_p = 0.2$. In addition, we take the beam dimensions for the flange as $\eta = 5$ and $\lambda = 2$.

Using the above parameters, the dimensionless load–deflection characteristics for both the deformation without crack growth and the deformation with crack growth modes are drawn in Fig. 9. A bifurcation point that describes the transition from type I to type II occurs at point T when $\bar{p} = \bar{p}_t$.

The bifurcation load $\bar{p}_t$ does not depend on η because eqns (70)–(72) are independent of η. However, $\bar{p}_t$ will be dependent on other parameters such as ς, r, λ and μ. We will consider only the effect of geometric parameters on the bifurcation load and the force–

Table 1. Material constants for mild strength steel (ship steel)

Flow stress σ_0 (MPa)	Plastic modulus E_p (MPa)	Specific work of fracture R (kJ m^{-2})
300	840	250

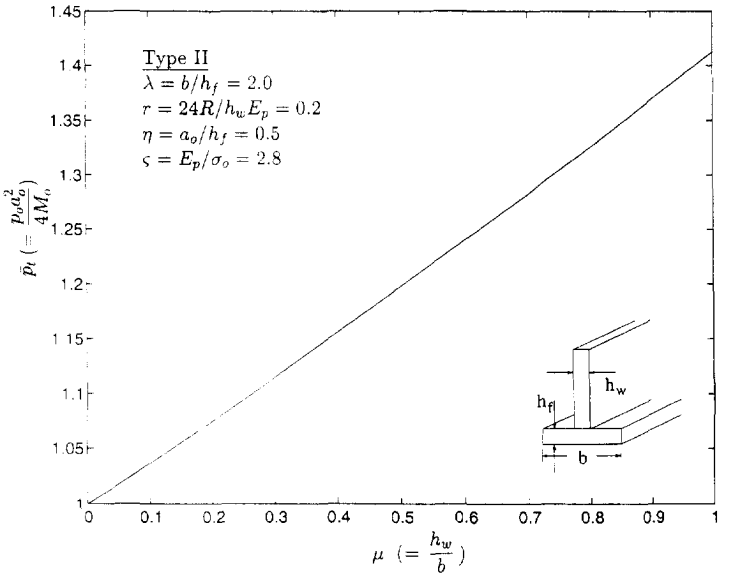

Fig. 10. Bifurcation load $\bar{p}_t$ versus ratio of tear width to flange width $\mu(= h_w/b)$.

deflection characteristics in type II. In particular, we keep the relative dimensions of the flange at $\eta = a_0/h_f = 5$ and $\lambda = b/h_f = 2$ fixed and vary μ, the ratio of the width of the tear and flange, in the range $0 < \mu < 1$. The μ parameter also compares the thickness of the stiffener web (or width of tear region) with the width of the flange (effective plate thickness).

Figure 10 shows that there is roughly a linear increase in the bifurcation load $\bar{p}_t$ as the relative magnitude of the width of the tear to the flange, μ, increases. When $\mu = 0$, $\bar{p}_t = 1$, i.e. there is no stiffener ($h_f = 0$) and the flange simple deforms without tearing (type I behavior). One can distinguish this from another limiting case when the tear region and width of the flange are equal, $\mu = 1$; because the width of the flange is an effective plate width, we must restrict the analysis to the region $0 < \mu < 1$. A maximum value for the bifurcation load occurs when $\mu = 1$. For the chosen material and geometric parameters, the bifurcation load may be as much as 50% greater than the limit load.

The variation in the load–deflection characteristics of the flange during crack growth is shown in Fig. 11 for several μ values. The linearly decreasing function which describes

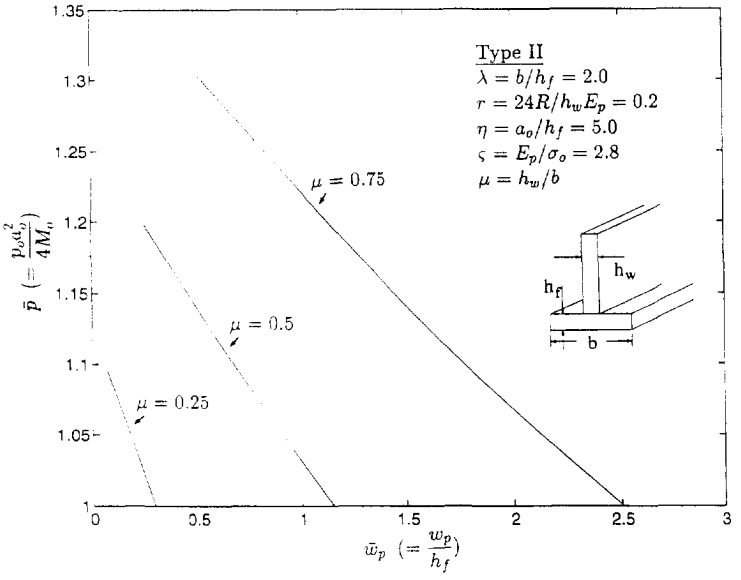

Fig. 11. Load–deflection characteristics as the crack grows for several values of $\mu(= h_w/b)$.

load–deflection characteristics of the flange as the crack propagates has a steeper gradient for smaller values of μ. This is expected because a smaller value of μ implies an increasing flange width for a fixed web thickness and the lower flange will be stiffer with a greater value of the effective width.

7. CONCLUDING REMARKS

A local tearing mechanism that can be used to examine the peeling of a stiffener from a plate is presented. A rigid, linear strain-hardening beam analysis is used to calculate the load–deflection characteristics of the transversely-loaded flange (effective width of stiffened plate). It is shown that the flange deforms in two ways with increasing values of load amplitude: deformation without crack growth (type I): and deformation with crack growth (type II). A deformation profile that incorporates two plastic unloading regions is proposed for type II behavior. The region of crack growth deforms with constant curvature, while the region adjacent to it has a plastic zone size and curvature that are determined from the type I analysis.

A bifurcation point occurs when the flange response changes from deformation without crack growth to deformation with crack growth. This bifurcation point is independent of the initial crack length, but a parametric study shows that the bifurcation load increases approximately linearly with an increasing ratio of the web thickness to flange width. This means that the crack is less likely to propagate when larger values for the effective plate width are assumed. The effective width of the stiffened plate is thus an important parameter in the detachment of the plate from the stiffeners.

Acknowledgements—The work reported herein was supported by the ONR contract No. N000 14-89-C-0301 to the Massachusetts Institute of Technology. Special thanks are extended to Frank McClintock, Tom Wierzbicki and Traci Williams for their help on various aspects of the paper.

REFERENCES

Atkins, A. G. and Liu, J. H. (1993). A single curl failure of metal plate in ship grounding. Joint MIT-Industry Program on Tanker Safety, Massachusetts Institute of Technology, *Technical Report No. 17*, May.

Atkins, A. G. and Mai Y.-M. (1985). *Elastic and Plastic Fracture*. John Wiley, New York.

Chang, M. D., Devries, K. L. and Williams, M. L. (1972). The effects of plasticity in adhesive fracture. *J. Adhesion* **4**, 221–231.

Haythornwaite, R. M. (1961). Mode change during the plastic collapse of beams and plates. In *Proceedings of the 7th Midwestern Mechanics Conference on Developments in Mechanics* (eds J. E. Lay and L. E. Malvern), Vol. 1, Plenum Press, NY, pp. 203–215.

McClintock, F. A. (1994). Fully plastic fracture mechanics for welded T-Joints. Joint MIT-Industry Program on Tanker Safety, Massachusetts Institute of Technology, *Technical Report No. 26*, February.

Youngdahl, C. K. (1991). A modal approximate method for strain-hardening beams. *Int. J. Impact Engng* **11**, 61–75.